Targeted disruption of the neurofibromatosis type-1 gene leads to developmental abnormalities in heart and various neural crest-derived tissues

Camilynn I. Brannan, Archibald S. Perkins,[1] Kristine S. Vogel, Nancy Ratner,[2] Michael L. Nordlund,[2] Susan W. Reid, Arthur M. Buchberg,[3] Nancy A. Jenkins, Luis F. Parada, and Neal G. Copeland

Mammalian Genetics Laboratory, ABL–Basic Research Program, Frederick Cancer Research and Development Center, Frederick, Maryland 21702-1201 USA; [1]Department of Pathology, Yale University School of Medicine, New Haven, Connecticut 06437 USA; [2]Department of Anatomy and Cell Biology, University of Cincinnati College of Medicine, Cincinnati, Ohio 45267-0521 USA

The neurofibromatosis (*NF1*) gene shows significant homology to mammalian GAP and is an important regulator of the *ras* signal transduction pathway. To study the function of *NF1* in normal development and to try and develop a mouse model of NF1 disease, we have used gene targeting in ES cells to generate mice carrying a null mutation at the mouse *Nf1* locus. Although heterozygous mutant mice, aged up to 10 months, have not exhibited any obvious abnormalities, homozygous mutant embryos die in utero. Embryonic death is likely attributable to a severe malformation of the heart. Interestingly, mutant embryos also display hyperplasia of neural crest-derived sympathetic ganglia. These results identify new roles for *NF1* in development and indicate that some of the abnormal growth phenomena observed in NF1 patients can be recapitulated in neurofibromin-deficient mice.

[*Key Words*: Neurofibromatosis; NF1; *Ras*; ES cells; transgenic mice]

Received February 8, 1994; revised version accepted March 25, 1994.

Von Recklinghausen neurofibromatosis or neurofibromatosis type 1 (NF1) affects 1 in 3500 humans, making it one of the most common inherited human diseases. NF1 is inherited as an autosomal dominant disease with the most common phenotypic manifestations resulting from abnormalities of neural crest-derived tissues (Riccardi 1981, 1991; Riccardi and Eichner 1986). These abnormalities include benign tumors of the peripheral nerves composed mainly of Schwann cells and fibroblasts (neurofibromas), tumors of the iris (Lisch nodules), and hyperpigmentation of melanocytes (café au lait spots). In addition, NF1 patients are at an increased risk for specific kinds of malignant disease, including neurofibrosarcoma, astrocytoma, pheochromocytoma and embryonal rhabdomyosarcoma (Bader 1986).

Although the clinical manifestations of NF1 are transmitted in an autosomal dominant fashion, it has been hypothesized that *NF1* mutations are recessive at the cell level. If true, NF1 would comply with the Knudson model devised to explain the inheritance of retinoblastoma (Knudson 1971), whereby one mutated and one normal allele are inherited, but tumors do not arise until the normal allele acquires a mutation as well. This model would place *NF1* in the class of tumor suppressor genes, which includes *RB*, *WT1*, *P53*, and possibly *APC*, whose encoded proteins control cell growth (Marshall 1991).

Evidence that *NF1* is a tumor suppressor gene is twofold. First, the majority of germ-line *NF1* mutations described thus far are predicted to produce no protein product (Gutmann and Collins 1993). Second, clonally derived malignant neurofibrosarcomas express nearly no detectable NF1 protein (Basu et al. 1992; DeClue et al. 1992), and one neurofibrosarcoma from an NF1 patient contains a somatic 200-kb deletion that eliminates the 5′ half of the normal *NF1* allele. Therefore, both alleles are defective in this tumor (Legius et al. 1993).

The *NF1* gene was identified in 1990 by positional cloning (Viskochil et al. 1990; Wallace et al. 1990). The human *NF1* gene spans >300 kb of genomic DNA and encodes an mRNA of 11–13 kb comprising ~50 exons, which is capable of encoding a 2818-amino-acid protein (for review, see Gutman and Collins 1993). The *NF1*-encoded protein, neurofibromin, has extensive homology with two negative regulators of Ras in *Saccharomy-*

[3]Present address: Jefferson Cancer Institute, Department of Microbiology and Immunology, Philadelphia, Pennsylvania 19107-5541 USA.

ces cerevisiae, IRA1 and IRA2 (Ballester et al. 1990; Buchberg et al. 1990; Xu et al. 1990a). NF1 and IRA share homology with the domain of mammalian GAP that encodes its GTPase-activating function. This GAP domain negatively regulates Ras by catalyzing the conversion of the active GTP-bound form of Ras to the inactive GDP-bound form (Hall 1990). The GAP-like domain of neurofibromin can complement the loss of the yeast RAS-binding protein IRA (Ballester et al. 1990; Xu et al. 1990b), and can interact with, and stimulate, the GTPase activity of Ras in vitro (Martin et al. 1990).

Ras is well known for its role in the control of cell proliferation but it can also induce morphological differentiation in PC12 cells (Bar-Sagi and Feramisco 1985; Noda et al. 1985). The biological response of cells to Ras-mediated signals is thought to reflect the intrinsic properties of a given cell type rather than an inherent property of the Ras protein itself. It also appears that *NF1* has a complex role in signal transduction, depending on the cell type. Analysis of schwannoma cell lines from neurofibromatosis patients indicates that low levels of neurofibromin, and the subsequent reduction in GAP-like activity, are associated with an increase in Ras–GTP, resulting in the stimulated growth of these lines (Basu et al. 1992; DeClue et al. 1992). Normal GAP levels are found in schwannoma lines, indicating that neurofibromin is an important negative regulator of Ras function in schwannoma lines and is key to regulating cellular proliferation. In contrast, neuroblastoma and melanoma cell lines that lack neurofibromin do not show altered Ras–GTP levels (Johnson et al. 1993; The et al. 1993). This implies that the GAP-like activity of neurofibromin is not the sole regulator of Ras–GTP levels in these cell types and that its role may be independent of Ras, perhaps regulating a differentiation pathway.

The developmental expression pattern of NF1 protein has been analyzed in the rat (Daston and Ratner 1992) and the mouse (Huynh et al. 1994). Neurofibromin is uniformly distributed throughout embryonic days 8–11. At embryonic day 12, however, NF1 protein becomes enriched in a subset of tissues, including the heart, dorsal root ganglia, liver, metanephros, stomach lining, and bronchial tubes (Huynh et al. 1994). By day 16, neurofibromin is enriched in the cortical plate, dorsal root and sympathetic ganglia, and the central nervous system (Daston and Ratner 1992). This neuronal restriction continues into the adult where the protein is detectable only in the brain, spinal cord, peripheral nerve, and adrenal medulla (Daston et al. 1992; Golubic et al. 1992).

Two alternatively spliced *NF1* exons have been reported. One exon, exon 23a, is located within the GAP-related domain and encodes an additional 21 amino acids (Nishi et al. 1991). Using an antibody specific for this 21-amino-acid epitope, Huynh et al. (1994) demonstrated that this isoform is present at low levels from mouse embryonic day 8–11 but becomes highly enriched in the heart at day 12 before declining at embryonic day 13. In the adult mouse, this isoform is predominantly expressed in the brain as detected by RNA reverse transcriptase–polymerase chain reactin (RT–PCR) analysis (Nishi et al. 1991). The other alternatively spliced exon, exon 48a, is located near the carboxyl terminus of the protein and encodes an additional 18 amino acids. The expression pattern of this second isoform was analyzed by RNA RT–PCR in humans and found to be expressed at high levels in adult cardiac muscle, skeletal muscle, and bladder. High levels were also detected in fetal heart (Gutmann et al. 1993). Additionally, this isoform was detected in muscle tissues from other vertebrate species, including mice. The expression profile of both alternatively spliced forms of NF1 includes embryonic and adult heart, suggesting a role for neurofibromin in normal cardiac development.

Neurofibromin is highly conserved throughout evolution: The mouse *Nf1* protein is >98% identical with the human protein (Bernards et al. 1993). This conservation suggests that a mouse model system might be useful for elucidating the role of *NF1* in development and disease. To this end, we have used gene targeting in embryonic stem (ES) cells to generate mice that carry a null mutation at *Nf1*.

Results

Generation of mice with a mutated Nf1 *gene*

To construct a replacement type *Nf1* targeting vector (Thomas and Capecchi 1987), a pMC1neo/poly(A) cassette (Thomas and Capecchi 1987) was inserted in the opposite transcriptional orientation into exon 31 of an *Nf1* genomic fragment, providing 7.1 kb of flanking homology at the 5′ end and 1.5 kb of homology at the 3′ end (Fig. 1A). Exon 31 was chosen as the site for mutation because several point mutations were found in this exon in NF1 patients (Cawthon et al. 1990). For negative selection against random integration events, a viral thymidine kinase gene, under the control of the pMC1 promoter (Thomas and Capecchi 1987) was included at the 3′ end of the vector (Fig. 1A). The targeting vector was linearized in plasmid sequences and electroporated into CCE–ES cells (Robertson et al. 1986). ES cell clones were doubly selected in G418 and FIAU, and targeted clones were identified by PCR analysis using an oligonucleotide primer from the *neo*^{r} gene and a primer from *Nf1* exon 33 (see Materials and methods). Homologous recombination events were further confirmed by Southern blot analysis using probes that flanked the targeting vector (Fig. 1A,B). Two targeted ES clones, 10f and 38a, were injected into C57BL/6J blastocysts and transferred into the uteri of pseudopregnant recipients. Chimeric male mice derived from both cell lines were each bred to C57BL/6J and 129/SvJ females and shown to transmit the *Nf1* mutation through their germ line. The results described in this study were indistinguishable for mouse lines derived from ES clones 10f and 38a.

Mice heterozygous for the mutation, designated *Nf1*^{Fcr}, had no apparent phenotype when compared with their wild-type littermates. Of 528 mice derived from an outcross of heterozygous males to wild-type females, 265 mice were wild type and 263 were heterozygous, indi-

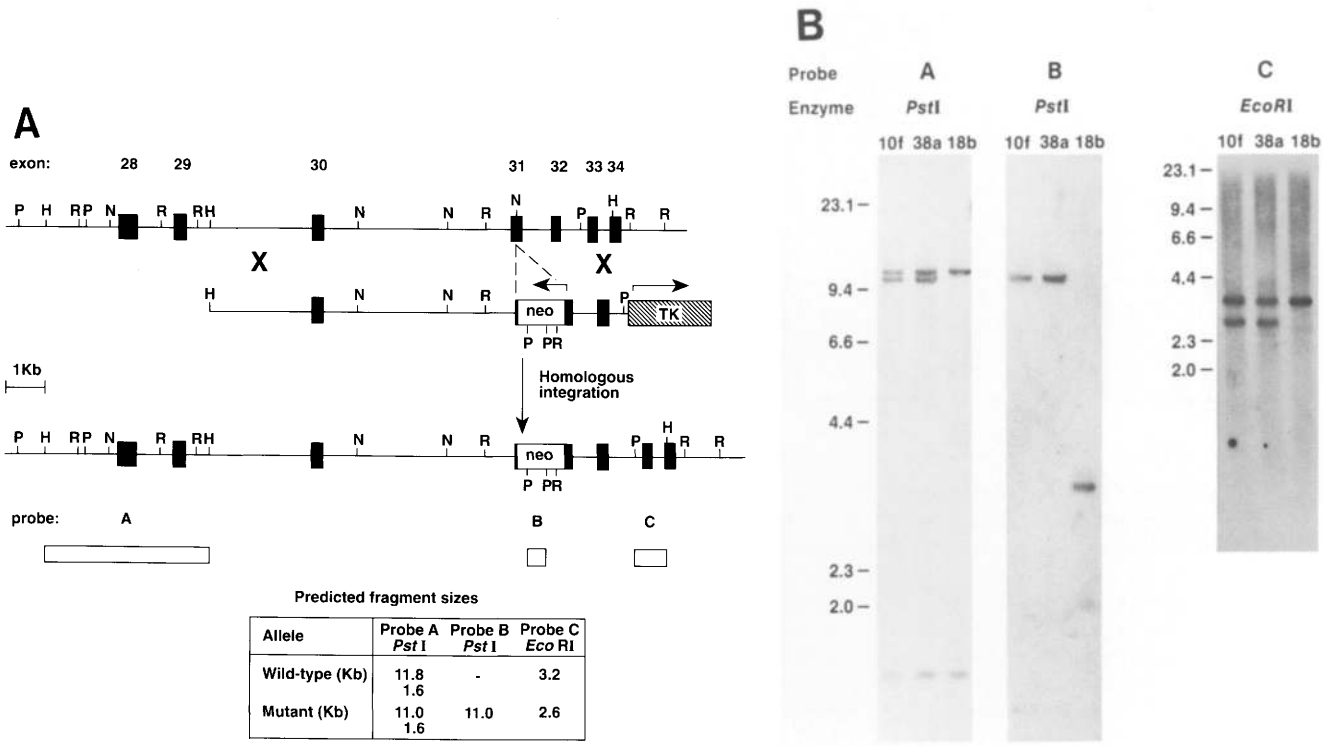

Predicted fragment sizes

Allele	Probe A *Pst* I	Probe B *Pst* I	Probe C *Eco* RI
Wild-type (Kb)	11.8 1.6	-	3.2
Mutant (Kb)	11.0 1.6	11.0	2.6

Figure 1. Targeted disruption of the *Nf1* locus. (*A*) Homologous recombination at the *Nf1* locus. The *top* line represents the structure of the region of the *Nf1* gene containing exons 28–34. Exons are shown as black boxes. The middle line represents the targeting vector in which the 1.1-kb pMC1neo/poly(A)$^+$ cassette has been inserted into the *Nco*I site of exon 31 and a viral thymidine gene, under the control of the pMC1 promoter, which has been placed at the 3′ end. Arrows indicate the direction of transcription of the *neo*^{r} and *tk* genes. In the *bottom* line is the predicted structure of the locus following targeted integration of the replacement vector. Homologous recombination events were confirmed by probing Southern blots of ES cell clones with probes A, a 4-kb *Hind*III fragment; B, a 680-bp Neo *Pst*I fragment; and C, a 1-kb *Pst*I–*Hin*dIII fragment. The expected sizes of diagnostic restriction fragments are given in the box. (H) *Hin*dIII; (P) *Pst*I; (R) *Eco*RI; (N) *Nco*I. (*B*) Southern blot analysis of ES cell clones transfected with the targeting vector. DNA from Neo^r FIAU^r ES clones were digested with *Pst*I or *Eco*RI, blotted, and hybridized with either probes A, B, or C. The clones 10f and 38a contain bands diagnostic of homologous recombination at the *Nf1* locus. Clone 18b represents a random integration event.

cating that there is no reduction in early survival of mice containing one copy of the *Nf1*^{Fcr} allele. In addition, heterozygotes, aged up to 10 months, have yet to display any abnormalities similar to those observed in human NF1 patients.

Homozygous Nf1^{Fcr} *mice die in utero*

No liveborn homozygous mutant mice were produced in heterozygous intercrosses, indicating that the *Nf1*^{Fcr} mutation is lethal during embryogenesis. To determine the time of death, embryos at 11.5–14.5 days postcoitum (dpc) derived from the intercross were analyzed histopathologically and their *Nf1* genotype determined (see Materials and methods). The results of this analysis are shown in Figure 2. Necrotic homozygous mutant embryos were found as early as 11.5 dpc; however, live homozygous mutant embryos could still be observed as late as 13.5 dpc. By 14.5 dpc no viable homozygous mutant embryos were observed. These results indicate that the *Nf1*^{Fcr} mutation is lethal by 14.5 days in development.

The Nf1^{Fcr} *mutation represents a null allele*

The majority of human germ-line *NF1* mutations characterized to date are predicted, or have been shown, to produce little or no neurofibromin. To determine whether the *Nf1*^{Fcr} mutation is capable of producing neurofibromin, RNA from both wild-type and homozygous mutant embryos was analyzed by Northern analysis for *Nf1* expression. Although a faint signal at 11–13 kb was consistently detected in wild-type embryo RNA, no transcripts of this size were detected in mutant RNA (data not shown). Further analysis using a more sensitive RNA RT–PCR approach, which made use of a series of primers located upstream of the *neo*^{r} gene insertion, gave inconclusive results. In homozygous mutant embryo RNAs, a weak signal could be detected with some primer pairs but not with others (data not shown). Because of these ambiguous RNA results we decided to test directly for the neurofibromin protein by Western blotting (Datson et al. 1992). The 220-kD neurofibromin protein was present in wild-type embryo extracts and was consistently present in heterozygous littermate embryo ex-

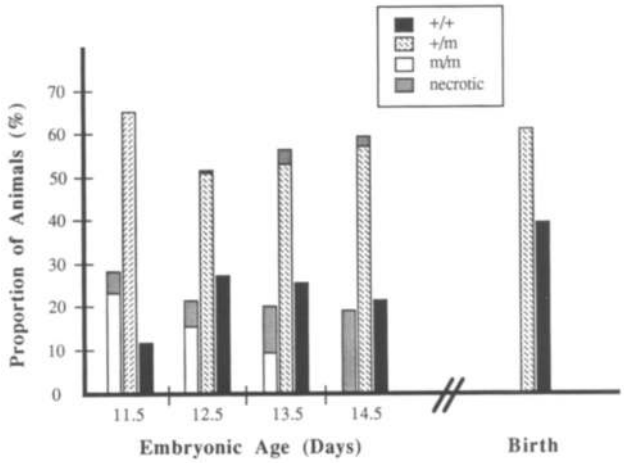

Figure 2. Genotype and phenotype of *Nf1*^{Fcr} mutant embryos at varying gestational ages. Cumulative genotype data from analysis of 504 embryos derived from 69 litters were sorted by gestational age. The percentage of embryos of each genotype is plotted. Wild-type embryos (solid boxes); heterozygous animals (crosshatched boxes); homozygous mutant animals (open boxes). Overtly necrotic embryos are indicated by stippled boxes. Slashed *x*-axis indicates that this analysis did not include embryos beyond 14.5 days of gestation. The genotypes of live-born mice are included for comparison.

tracts, albeit at reduced levels (Fig. 3A). However, we were unable to detect neurofibromin in extracts from homozygous mutant embryos (Fig. 3A). To enhance the sensitivity of our assay, neurofibromin was first concentrated by immunoprecipitation then submitted to Western blotting. Whereas neurofibromin was readily detectable in 200 μg of control wild-type embryo extract, no neurofibromin was detected in 2 mg of homozygous mutant embryo extract (data not shown). Because the antibody used in these experiments recognizes an amino-terminal domain of neurofibromin, truncated mutant Nf1 protein, if present, should have been detected. These results suggest that the *Nf1*^{Fcr} mutation is a null allele.

Western analysis was also carried out on extracts of brain from wild-type and heterozygous adult mice. As in the embryo, heterozygous mice contained reduced levels of neurofibromin as compared with wild-type mice (Fig. 3B). Immunostaining of mouse embryos and adult mouse brains have supported these results. Although immunostaining of wild-type and heterozygous mice with anti-neurofibromin antibody showed approximately a two-fold reduction in neurofibromin, the pattern of neurofibromin distribution was the same in mice of both genotypes (data not shown).

Abnormal cardiac development in Nf1^{Fcr} *mutant mice*

At 12.5 dpc, homozygous mutant embryos can be distinguished because of an enlarged head and chest bulge, pale liver, and small eyes (Fig. 4). Much of the apparent hypertrophy is attributable to tissue edema, distended lymphatics, and veins [e.g., Fig. 6D (asterisk), below] and pericardial and pleural effusions. This generalized edema, together with systemic vascular congestion, suggested cardiac failure as a significant contributory factor to midgestational demise in mutant embryos.

At 13.5 dpc, the mutant hearts are globular, hypoplastic, and show disoriented and poorly developed myocardial fibers (Fig. 5). Relative to heterozygous littermates, the mutant embryos exhibit a significant ventricular septal defect (VSD; Fig. 5, cf. B with A and D with C), which likely reflects the lack of downward growth of the ventricles. Whereas the heterozygotes have a virtually complete and intact interventricular septum (IVS) comprised of both muscular and membranous portions, the mutants are less well developed with only a rudimentary septum near the apex that was exclusively muscular.

In normal littermates at 13.5 dpc, the aorta (Ao) and pulmonary artery (PA) have completely separated and emanate from the left and right ventricles (LV and RV), respectively (Fig. 5A,E). The mutants, however, have a common root of the Ao. and PA [the truncus arteriosus (TA)] departing from the conus cordis of the RV (Fig. 5B,I,F). As the truncus proceeds cephalad, it divides into two channels, the PA and the Ao, which are not fully

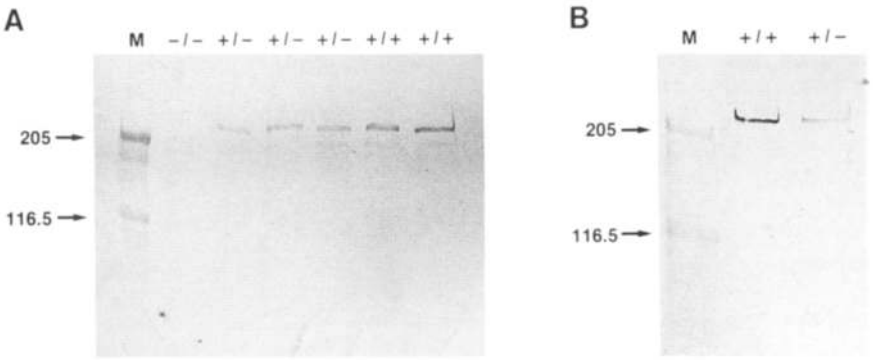

Figure 3. Western blot analysis of *Nf1*^{Fcr} mutant mice. Extracts from *Nf1*^{Fcr}/*Nf1*^{Fcr}, +/*Nf1*^{Fcr} and +/+ 12.5-dpc embryonic heads (200 μg) (*A*) or +/*Nf1*^{Fcr} and +/+ adult heads (*B*) were fractionated on a 7% acrylamide gel and transferred to membrane. The blot was probed with a polyclonal antibody made to the amino-terminal region of neurofibromin (Daston et al. 1992), and neurofibromin was visualized by an alkaline phosphatase-conjugated secondary antibody. The faint band at 200 kD in *A* was not present in all experiments and likely represents a degradation product of neurofibromin. The migration of prestained molecular markers (M) is shown at the *left* (numbers represent kD).

Figure 4. Wild-type (Wt) and homozygous mutant (M) embryos at 12.5 dpc.

separate and are joined in a common external sheath (Fig. 5H,G). These features indicate delayed and perhaps fundamentally abnormal cardiac development in mutant mice that was likely accompanied by significant cardiac dysfunction.

Additional abnormalities were seen in the cardiac valves in the mutants. At 13.5 dpc, the atrioventricular canal (AVC) in the mutant hearts was composed of loosely arranged endothelial cells that lacked the typical cellular density seen in the hearts of control littermates. Normally by 13.5 dpc, the endocardial cushions of the AVC have fused to divide the canal into right and left channels. Valve leaflets are typically evident, which are thought to be formed by infiltrating cardiac myocytes that later degenerate, giving rise to the fibrous valve found in adult animals. This cellular migration imparts a densely cellular microscopic appearance to the valve, with most of the density concentrated at the cusps (Fig. 5A, arrows). In contrast, the 13.5 dpc mutant endocardial cushion retains the loose, myxoid appearance seen at 12 dpc (Fig. 5B, arrows), even though it does merge and divides the AVC into left and right channels (Fig. 5G–I, LAVC and RAVC). These observations suggest that myocyte infiltration has failed to occur in the mutant. The mutant cushion tissue is also considerably larger than

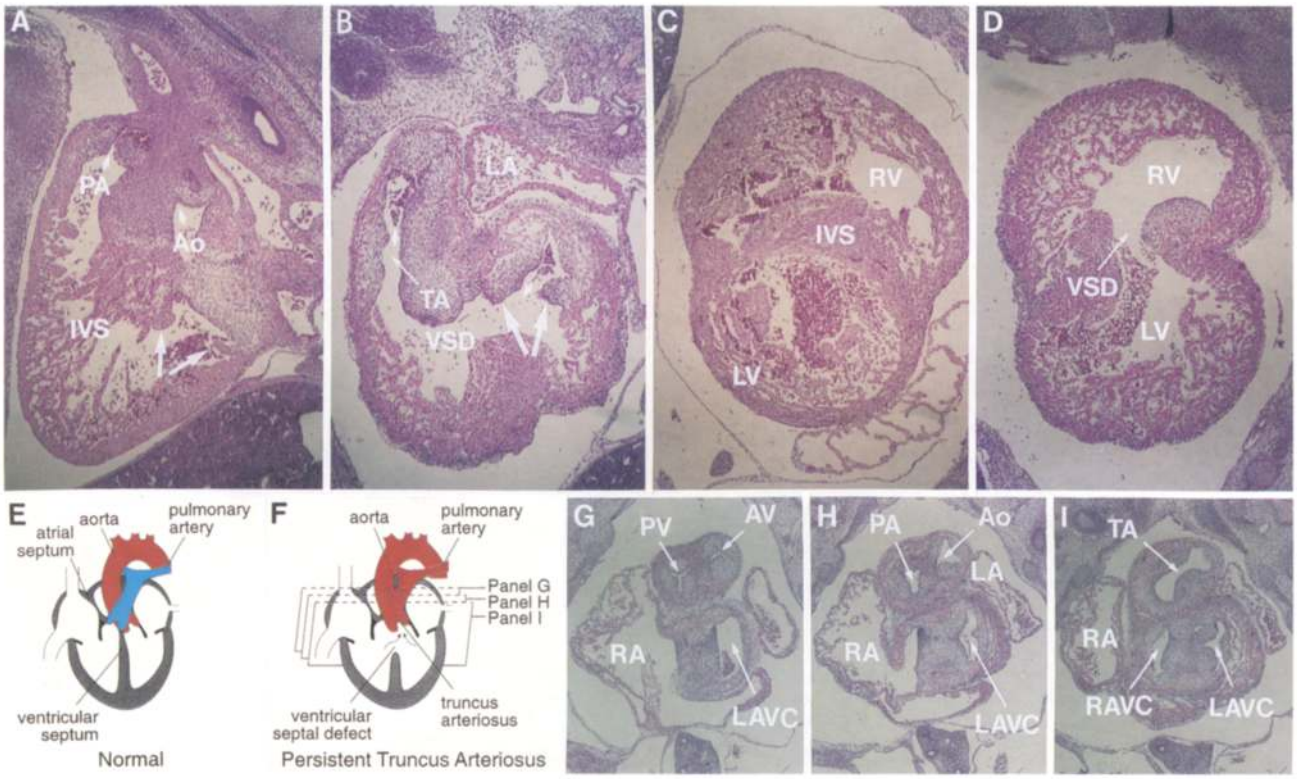

Figure 5. Malformation and developmental delay in cardiogenesis in homozygous mutant embryos. H+E-stained sagittal (*A,B*) and frontal (*C,D,G–I*) views of 13.5-dpc mutant (*B,D,G–I*) and normal (*A,C*) hearts. *A* and *B* show that while the normal heart (*A*) has an interventricular septum (IVS), and separated PA and Ao, the mutant (*B*) has a ventricular septal defect (VSD) and an incompletely divided truncus arteriosus (TA). Arrows indicate the leaflets of the mitral valve, which in the mutant remain poorly condensed. (LA) Left atrium. Short arrows in *B* indicate the direction of blood flow. (*C,D*) The VSD between the RV and LV in the mutant heart (*D*). The drawings in *E* and *F* illustrate the characteristic features of the mutant heart compared with a normal heart at this stage of development. They also show the planes of section for *G–I*, which cut through the TA in sequentially more caudal levels and show that whereas the PA and Ao and their respective valves, the pulmonary valve (PV) and the aortic valve (AV), are present, they emerge from a common TA that emanates from the right ventricle. Also indicated are the right atrium (RA), the right atrioventricular canal (RAVC), the left atrium (LA), and the left atrioventricular canal (LAVC). Original magnification: (*A–D*) 6.25×; (*G–I*) 4×.

controls at 13.5 dpc (Fig. 5A,B), which may reflect continued proliferation of this tissue or failure of the endothelial cells that comprise the structure to undergo apoptosis, or tissue edema.

Delay in renal, hepatic, and skeletal muscle development

Examination of several visceral organs and systems in the mutant embryos reveals an 18- to 24-hr delay in development. This is particularly evident in the renal, hepatic, and skeletal muscle systems. In the metanephros, the delay is manifested by a retardation of its cephalad repositioning and a reduced number of glomeruli. At 13.5 dpc, the mutant embryos exhibit hypoplasia of the liver, accompanied by focal necrosis and hemorrhage. In addition, skeletal muscle throughout the body of mutant embryos is also hypoplastic relative to normal counterparts (Fig. 6). The musculature of the stomach and the three layers of the abdominal musculature (Fig. 6A,B), as well as the muscles of the shoulder girdle (Fig. 6C,D), are markedly thinner in the mutant. These findings indicate that the *Nf1* mutation results in developmental delay and hypoplasia that affect a number of organ systems.

Detailed microscopic examination of the other systems, organs, and structures in the embryo did not reveal any other significant anomalies other than an apparent exencephaly that was observed in ~6.3% of homozygous mutant embryos.

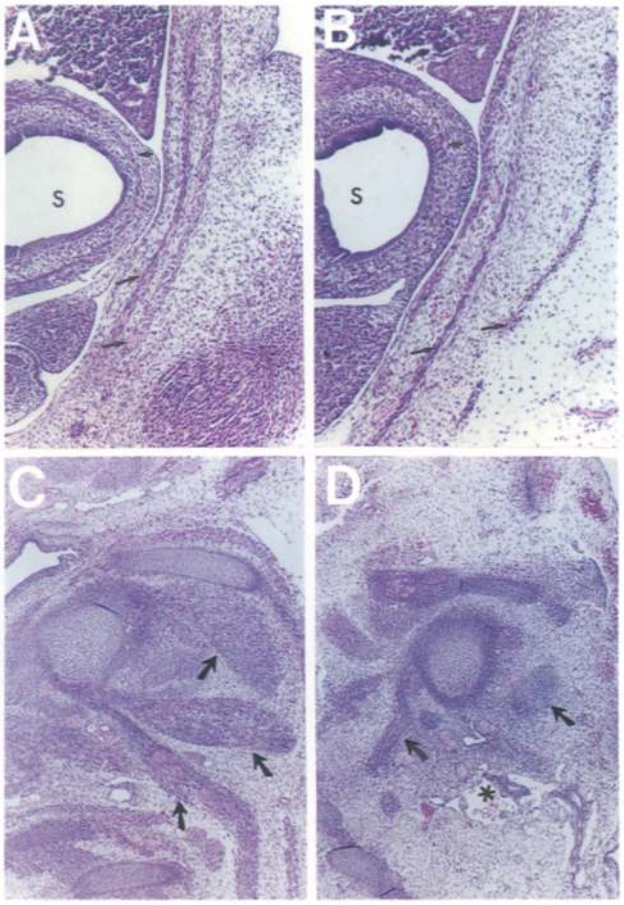

Figure 6. Hypoplastic musculature in homozygous mutant embryos. H+E-stained sagittal sections of wild-type (*A*) and mutant (*B*) embryos showing delayed development of abdominal wall (long arrows) and smooth muscle in the stomach (S) wall (short arrow). In addition, the three layers of the abdominal wall musculature are more widely spaced. The hypoplasia of the skeletal muscle is evident in the mutant limb girdles (*D*, arrows) as compared with those in the wild type (*C*). *D* also displays a distended lymphatic vessel due to tissue edema (*). Original magnification, 12.5×.

Hyperplasia of the prevertebral and paravertebral sympathetic ganglia in homozygous mutant mice

A striking and potentially informative alteration found in mutant embryos is an overgrowth of the paravertebral and the prevetertebral sympathetic ganglia. The sympathetic ganglia arise from the neural crest and reside in the retroperitoneum adjacent to, and in front of, the spinal cord, respectively. Normal 13.5-dpc embryos have discrete, circumscribed paravertebral sympathetic ganglia (circumscribed by arrows and outlined in Fig. 7A). Mutants exhibited ganglia that are two to three times the size in normal littermates and that appeared to extend abnormally (Fig. 7B). The neuronal identity of cells within the enlarged ganglia was confirmed with immunostains for the neuronal markers synaptophysin, a synaptic vesicle protein (Fig. 6C), and neurofilament, as well as with silver stains (data not shown). Hematoxylin and eosin (H+E)-stained sections of mutant sympathetic ganglia show large cell bodies with big nuclei, prominent nucleoli, and the fine dendritic morphology characteristic of neurons (Fig. 7B, inset). Stains for an enzyme involved in the biosynthesis of catecholamines, tyrosine hydroxylase, was positive, further indicating the identity of these cells as sympathetic neurons (data not shown). A similar overgrowth of the prevetebral sympathetic ganglia was also observed (data not shown).

The increased size of these ganglionic anlagen appeared to be attributable to increase in cell number rather than cell size. Dissection of the paravertebral sympathetic chains from 12.5-dpc embryos confirms these results. The chains derived from mutant embryos are much larger and more cohesive as compared with wild-type littermates. Dissociation and culturing of the cells for 24 hr shows 2.3 times more neurons in the mutants (Table 1). In addition, dissection, dissociation, and culturing of the superior cervical ganglia derived from 12.5-dpc littermates demonstrates that the mutant cultures contained 1.95–3.3 times more neurons than controls (Table 1).

Numeration of mitotic figures on H+E-stained slides indicated a 50% increase in mitotic index in the mutant sympathetic ganglia. Nuclear debris, suggestive of apoptotic cells, were present with similar frequency in mutant and control ganglia. These findings are consistent with an increased rate of mitosis in the mutant as being

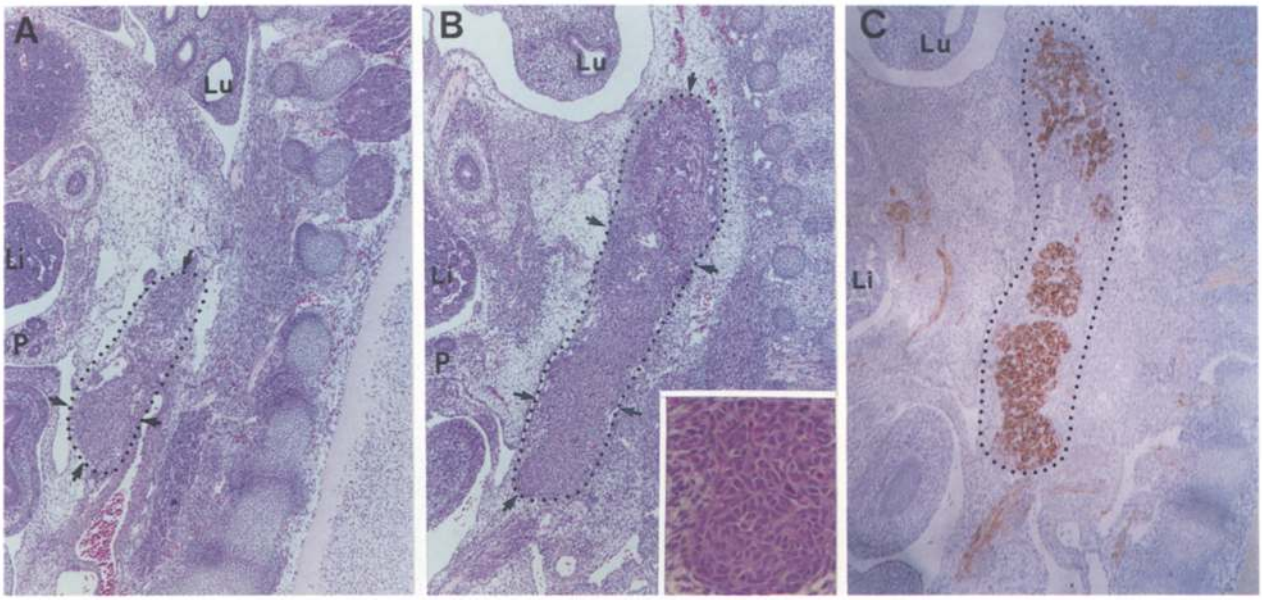

Figure 7. Homozygous mutant embryos display hyperplasia of the paravertebral sympathetic neurons. (*B,C*) The 13.5-dpc mutant; (*A*) control embryo. (*A,B*) H+E-stained sagittal sections. Arrows and outline demark the extent of growth of the sympathetic chain. Also indicated are lung (Lu), liver (Li), and pancreas (P). (*Inset* in *B*) An enlargement of an area of the mutant sympathetic ganglia, showing cells with large cell bodies containing big nuclei and prominent nucleoli, characteristics of neurons. (*C*) Immunoperoxidase staining of a nearby section with anti-synaptophysin antisera. Represented are the sections at which the paravertebral ganglion is the largest.

the cause of the observed hyperplasia. Other potentially contributory mechanisms, such as increased recruitment or a larger initial migration from the neural crest, cannot be ruled out at present.

Other ganglia were inspected on H+E-stained slides and appeared normal in size in the homozygous mutant embryos. In addition, two other neural crest-derived ganglia were dissected and trypsinized at various time points of development and exhibited no difference in neuronal size or number: Dorsal root ganglia were analyzed at 12, 12.5, and 13.5 dpc and trigeminal ganglia at 11.5, 12, and 12.5 dpc. Finally, the nodose ganglia, a placode-derived ganglia, was also found to have apparently normal neurons at 12 and 12.5 dpc.

Table 1. *Overgrowth of sympathetic neurons derived from* $Nf1^{Fcr}/Nf1^{Fcr}$ *mutants*

Experiment	Ganglia type[a]	Genotype	Neuron no.[b]	Ratio[c]
1	SCG	+/−	1224	
	SCG	−/−	2387	1.95
2	SCG	+/−	262	
	SCG	−/−	864	3.30
3	SyG	+/−	2282	
	SyG	−/−	5157	2.30
4	SyG	+/−	881	
	SyG	−/−	2004	2.27

[a](SCG) Superior cervical ganglia; (SyG) paravertebral sympathetic chains from trunk.
[b]Number of cells with neuronal morphology after 24 hr in culture.
[c]Ratio of neurons in −/− cultures compared with +/−.

Discussion

To better our understanding of the role of NF1 in normal development and disease, we have created mice that carry a null mutation at the *Nf1* locus induced via homologous recombination in ES cells. We have determined that homozygous mutant embryos died by 14.5 days in development. So far, heterozygous mutant mice have not developed any obvious abnormalities. However, in humans, NF1 is an autosomal dominant disorder. A number of possible explanations may account for this apparent discrepancy. First, the difference in life span and total cell number in humans as compared with mice may be of significance. If a second mutational event is required for development of NF1-like disease, a reduced target size in the context of a reduced time window may impede the onset of the disease in mice. Further aging of heterozygous mice coupled with exposure to mutagens may reveal an increased susceptibility of the mutant mice. It is also possible that mice may not be capable of developing neurofibromas or other developmental abnormalities observed in humans. Finally, it is possible that host-modifying genes affect the severity of NF1 disease. If this is the case, it may be necessary to cross the mutation onto a different strain background to observe the disease.

Heart defect

The cause of death of homozygous mutant embryos is

likely attributable to cardiac dysfunction. We base this conclusion on the many abnormal morphologic features consistent with this interpretation, including systemic edema, dilatation of the venous and lymphatic systems, and severe abnormalities of the heart. Whereas cardiac dysfunction is an obvious cause for these findings, the small size of the dying embryos precludes functional assessment of cardiac function in vivo; therefore, additional causes of hydrops, such as hypoproteinemia or renal dysfunction, must be considered. Although developmental delay could account for some aspects of the abnormal mutant hearts, a fundamental defect in cardiac development is also suggested by the histopathological results.

The severity of the malformations observed in the mutant embryo hearts indicate that neurofibromin has an important function in cardiac organogenesis and perhaps myocardial function. The abnormalities are multiple and complex and include overall hypoplasticity, and disoriented and poorly developed myocardial fibers, as well as a ventricular septal defect attributable to insufficient ventricular growth, and abnormalities in valve leaflet formation. The severity and the timing of the cardiac defects is intriguing in light of new data regarding the expression profile of neurofibromin. For example, Huynh et al. (1994) have demonstrated recently that an isoform of NF1 containing 21 additional amino acids within the GAP homology domain shows dramatic changes in levels during development: Expression is low at 11 dpc, peaks in the heart at 12 dpc, and declines by 13 dpc. This peak of expression in the heart is at precisely the stage in embryogenesis where the major heart defects in Nf1-deficient mice are observed. In addition, an alternatively spliced isoform of NF1 located in the carboxy-terminal end of the protein has recently been detected in fetal cardiac muscle in addition to adult muscle (Gutmann et al. 1993). Although it has not yet been confirmed that a protein encoding this isoform is produced in vivo, it is clear that the fetal heart is home to the two rare isoforms of neurofibromin. This information, together with the severe heart defects in embryos lacking *Nf1*, strongly argues that neurofibromin is essential for normal cardiac development.

In addition to the above abnormalities, hearts derived from homozygous mutant embryos contain a common departure of Ao and PA from the RV and incomplete separation of these two outflow vessels. This defect, called persistent truncus arteriosus, is commonly seen in congenitally anomalous human hearts. Interestingly, persistent TA can be induced in the developing chick by ablation of neural crest cells from the level of somites 1–3 (Kirby et al. 1983). From chick–quail chimera studies it has been established that the neural crest contributes to the ectomesenchymal cells that are involved in dividing the TA into PA and Ao, as well as in the formation of the pulmonary and aortic valves (Kirby et al. 1983). The caudal extent of migration appears to be the conus cordis, so that neural crest-derived cells do not contribute to the formation of the valves in the AVC. It is unlikely that lack of neurofibromin results in a complete block of neural crest migration into the heart, as in the mutant the truncus divides into two vessels, and the pulmonary and aortic valves are present. But the similarity of the phenotype observed in the mutant mice—common outflow tract and ventricular septal defect—to that seen with ablation of neural crest cells from the level of somites 1–3 in the chick, suggests that neurofibromin might play an important role in the migration or functional capacity of these neural crest-derived cells.

Although cardiac abnormalities were observed in all homozygous mutant *Nf1* mouse embryos, only a small number of human patients with NF1 have been diagnosed with congenital heart disease (Kaufman et al. 1972). This is most likely explained by the fact that human NF1 patients carry only one germ-line copy of the *NF1* mutation and most cells in the heart would thus be expected to be heterozygous for the mutation during this critical window of cardiac development in utero.

Renal, hepatic, and skeletal muscle defects

An 18- to 24-hr delay was evident in two organs, the liver and the kidney, as well as in the skeletal muscle system of homozygous mutant embryos. Again, this nicely reflects the pattern of neurofibromin expression in these organs. At 12 dpc, in addition to strong staining in the heart, the liver and metanephros are enriched in neufibromin (Huynh et al. 1994). However, whereas the heart contains mainly the isoform with the extra 21 amino acids derived from exon 23a, the liver and presumptive kidney are enriched in the isoform without these amino acids (Huynh et al. 1994).

The poorly developed skeletal musculature of the mutant embryos that we observed in the stomach and the limb buds may similarly be attributable to the isoform derived from an *Nf1* mRNA containing the alternatively spliced exon, 48a. It has been demonstrated that this isoform is present at high levels in adult skeletal muscle (Gutmann et al. 1993), but it is not known whether it is present in fetal skeletal muscle.

NF1 *as a regulator of growth*

Hyperplasia of the prevertebral and paravertebral sympathetic ganglia is a consistent feature of mutant 13.5-dpc embryos. Because of similarities, if not identities, in cellular origin, phenotypic markers, and even certain morphologic features, these lesions are analogous to the extra-adrenal pheochromocytomas that occur in patients with NF1. Although the demise of the mutant embryos before 14.5 dpc prevents the growth capacity and malignant potential of these lesions from being determined, this abnormal proliferation of neural crest-derived cells suggests an important role for the NF1 gene product in regulating growth in this cell type. The absence of hyperplasia of other peripheral nerves in homozygous mutant mice at the time of death could be attributable to the amount of time needed for these lesions to become evident but more likely reflects an intrinsic difference in the role of Nf1 in the different neuronal populations.

Does the hyperplasia of sympathetic ganglia in the mutant embryos implicate *Nf1* as a negative growth regulator in these cells? Sympathoadrenal precursors, after arising from the neural crest, initiate migration to form the sympathetic chain on day 10 pc (in the rat) and contain catecholamine synthetic enzymes by 12.5 dpc (Cochard et al. 1978). That a two- to threefold difference in size of the ganglia exists so soon after its initial establishment in mutant and wild-type embryos indicates a significant difference between mutant and wild-type cells in rates of cell division, cell death, and/or recruitment. The fact that nuclear debris, suggestive of apoptotic cells, was equally present in mutant and control ganglia is consistent with the view that the hyperplasia of sympathetic ganglia in mutant embryos is not the result of cellular protection from programmed cell death. This interpretation is further supported by the data from Wright et al. (1983), demonstrating that naturally occurring developmental neuron death does not begin in the rat SCG until after birth. Although our data are most consistent with an increased rate of mitosis in the mutant, other contributory mechanisms, such as increased recruitment or a larger initial migration from the neural crest must be ruled out.

In summary, we have created mice that carry a null mutation at the *Nf1* locus, which display some of the pathological features suggestive of human NF1 disease. Continued study of these mice may provide additional insights into our understanding of the role of NF1 in normal development and disease, which will be important for designing efficient therapeutic approaches to this important human genetic disease.

Materials and methods

NF1 *homologous recombination construct*

A 9.6-kb *Hin*dIII fragment was isolated from a C57BL/6 genomic phage using a partial NF1 cDNA as a probe (Buchberg et al. 1990). A 2-kb *Eco*RI–*Pst*I fragment containing exons 31 and 32 was subcloned into pUC18. The *Nco*I site in exon 31 was filled in and *Bam*HI linkers were added. A 6.6-kb *Hin*dIII–*Eco*RI fragment containing *Nf1* exon 30 was subcloned 5′ of the altered *Eco*RI–*Pst*I fragment. The 1.1-kb *Bam*HI Neo^r gene from pMC1neo/poly(A) (Thomas and Capecchi 1987) was subcloned into this *Bam*HI site in the opposite transcriptional orientation. Finally, the 9.6-kb *Hin*dIII fragment containing exons 30–32 with exon 31 disrupted by *neo*^{r} was subcloned into a plasmid containing pMC1Tk (Thomas and Capecchi 1987).

Electroporation and selection conditions

A total of 7×10^7 CCE–ES cells (Robertson et al. 1986) were grown up on mitomycin C-treated G418-resistant mouse embryo fibroblast (MEF) feeder cells, trypsinized, and resuspended in 3.2 ml of PBS, to which 120 μg of *Cla*I-digested replacement vector DNA was added. Four electroporations containing 0.8 ml each of this mixture were performed using a Bio-Rad Gene Pulsar at 250 V and 500 μF. The combined mixture was then aliquoted onto eight 10-cm dishes, four that contained STO feeder cells and four that contained MEF feeder cells. Twenty-four hours later, the culture medium was changed to include G418 at 250 μg/ml total (GIBCO) either with or without 2 μM FIAU. Fresh medium was added every day until 5 days after the electroporation, the medium was changed to 300 μg/ml of G418 for those cells on STO feeder cells and 200 μg/ml of G418 for those cells on MEF feeder cells. The FIAU was removed and 1000 U/ml of leukemia inhibiting factor (LIF) (GIBCO) was added. Colonies were picked either 9 days (those on STO feeders) or 12 days (those on MEF feeders) after electroporation. Portions of individual colonies were placed onto wells of a 24-well dish containing MEF feeders, and the remainder of each colony was pooled with portions of five other colonies and processed as described previously (Laird et al. 1991). Eight of 39 pools for 6 clones were positive by a PCR screen used to identify homologous recombination events. Individual PCR reactions identified the positive clones in each pool. Southern blot analysis was used to confirm that homologous recombination had occurred at both ends. Two positive clones were chosen for injection: 10f, selected on STO feeders and 38a, selected on MEF feeders. Both cell lines were subjected to a round of subcloning using 300 μg/ml of G418 on MEF feeders. Prior to injection, the cells were culture without G418 in the medium.

PCR conditions

For the screening of G418–FIAU-resistant colonies, one-third of the final volume of processed cells (5 μl) was added to 45 μl of PCR reaction mixture containing 5 μl of 10× reaction buffer (Perkin-Elmer Cetus), 400 ng of each oligonucleotide primer (NeoTkp, 5′-GCGTGTTCGAATTCGCCAATG-3′; NFexon 32, 5′-GAAGGACAGCATCAGCATG-3′), 0.5 units of *Taq* polymerase (Perkin-Elmer Cetus), and a mixture of dATP, dCTP, dGTP, and dTTP each at a final concentration of 250 μM. PCR was performed for 35 cycles using the following conditions: 94°C for 1 min, 55°C for 1 min, and 72°C for 2 min. Twenty microliters of the reaction was run out on an agarose gel, Southern blotted and probed with an NF1 cDNA probe (Buchberg et al. 1990).

To genotype the *Nf1* mice, a second set of *Nf1* oligonucleotide primers were used, both from exon 31 (NF31a, 5′-GTATTGAATTGAAGCACCTTTGTTTGG-3′ and NF31b, 5′-CTGCCCAAGGCTCCCCCAG-3′). PCR conditions were the same as above except for the following changes: 25-μl reactions were used containing 400 ng of each oligonucleotide primer: NeoTkp, NF31a, and NF31b. The entire reaction mixture was electrophoresed through a 1% agarose gel. PCR amplification of DNA from wild-type animals resulted in a 194-bp fragment; from homozygous mutant animals, a 340-bp fragment; and from heterozygous animals, both a 194-bp and a 340-bp fragment.

Generation of chimeric mice

Chimeras were generated essentially as described (Bradley 1987). ES cells (10–15) were injected into the blastoceol cavity of C57BL/6 blastocyst at 3.5 dpc. Injected blastocysts were transferred to the uterus of pseudopregnant recipients 2.5 days after mating with sterile males. Chimeras were identified by the agouti coat color. Male chimeras were mated with C57BL/6 females. Offspring with agouti coat color were genotyped by tail clip. Chimeras that transmitted the *Nf1* mutation through their germ line were mated with either C57BL/6J or 129/Sv females to establish lines.

Southern blot analysis

DNA was isolated from ES cells and embryos as described (Laird et al. 1991). DNA from tails was isolated as described by Siracusa et al. (1987). DNAs were digested to completion with an

excess of restriction endonuclease under reaction conditions recommended by the manufacturer (New England Biolabs). The digested DNAs were electrophoresed through 0.8% agarose gels and transferred to Zetabind (Cuno, Inc.). Conditions for prehybridization and hybridization were as described by Jenkins et al. (1982). Washes were done at 0.2× SSC, 0.1% SDS, at 65°C. Films were autoradiographed at −70°C using Kodak XAR film.

Anatomical, histological, and immunocytochemical analysis

Postimplantation embryos were recovered at various times of gestation. The morning that the vaginal plug was detected was considered as 0.5 dpc. Embryos were dissected and rinsed in PBS, and then fixed in 4% paraformaldehyde in PBS. Embryos were dehydrated and embedded in paraffin (Hogan et al. 1986). Embryos were sectioned at 4–5 μm thickness, mounted on gelatin-treated slides, and every fourth section was stained with H+E. Immunocytochemistry was done using unstained adjacent sections: a 1:100 dilution of a rabbit anti-synaptophysin (Dako) antibody was used after a 3 min trypsin digest; a 1:1000 dilution of a rabbit anti-neurofilament antibody (Sigma); a 1:1000 dilution of a rabbit anti-tyrosine hydroxylase antibody (Eugene Tech International, Inc.) was used after a 3-min trypsin digest; all were visualized after washing using the rabbit ABC Elite staining kit (Vectastain). Bodian staining was done according to Luna (1968). Photography was done using a Zeiss Axiophot Microscope.

Western blotting and immunoprecipitations

Western blotting and immunoprecipitation followed by Western blotting were carried out as described previously (Daston et al. 1992) except that the extracts were fractionated in 7% SDS-PAGE gels (Bio-Rad) and transfer was onto PVDF membranes using a three pH transfer system as described by Millipore (Technote 036). Blotting and immunoprecipitation results were confirmed in three separate litters of embryos, and in three pairs of age- and sex-matched adult mice. Results were the same using antibodies that recognize domains encoding amino acids 772–1085 and 2435–2745 of the neurofibromin sequence (nomenclature according to Marchuk et al. 1991). The specificity of these antibodies has been demonstrated previously (Daston and Ratner 1992; Daston et al. 1992). Immunostaining of fixed 30 mm frozen microtome sections of adult mouse cerebellum was carried out exactly as described in Nordlund et al. (1993).

Culturing of cells in vitro

Both superior cervical ganglia (SCG) were dissected from mutant and wild-type 12.5-dpc mice in Leibowitz-15 (L15) media containing 1× penicillin/streptomycin (GIBCO) using watchmaker's forceps. Both paraverteral sympathetic chains (SyG) corresponding to 10 or 14 vertebral segments were dissected from mutant or wild-type 12.5-dpc embryos in the above media using electrolytically sharpened tungsten needles. Following trypsinization at 37°C for 30 min (SyG) or 20 min (SCG) the ganglia were washed in culture medium (F14 with 10% heat-inactivated horse serum and 5% heat-inactivated fetal calf serum) and then gently triturated 8–10 times. The resulting single-cell suspension was plated onto 35-mm dishes that had been coated previously with polyornithine (0.5 mg/ml in 0.15 M borate buffer at pH 8.6, overnight) and then laminin (20 μl/ml in PBS, 4–6 hr at 37°C) in 2 ml of culture medium. The survival and initial neurite outgrowth of 12.5-dpc SCG and SyG neurons are not influenced by or dependent on the neurotrophins NGF, BDNF, NT-3, or NT-5 (K.S. Vogel, unpubl.). All cells with a neuronal morphology within a 5×5-mm grid in the center of each dish were counted 18–24 hr later.

Acknowledgments

We thank Dr. Liz Robertson for the gift of CCE–ES cells, and Jan Flynn, Bryn Eagleson, and Lisa Secrest for excellent technical assistance. This work was supported in part by the National Cancer Institute, Department of Health and Human Services under contract NO1-CO-74101 with ABL. C.I.B. was supported by a postdoctoral fellowship from the National Neurofibromatosis Foundation. A.S.P. was supported by a grant from the James S. McDonnell Foundation; and N.R. by a grant from the National Institutes of Health (NS28840).

The publication costs of this article were defrayed in part by payment of page charges. This article must therefore be hereby marked "advertisement" in accordance with 18 USC section 1734 solely to indicate this fact.

References

Bader, J.L. 1986. Neurofibromatosis and cancer. *Ann. N.Y. Acad. Sci.* **486:** 56–65.

Ballester, R., D. Marchuk, M. Boguski, A. Saulino, R. Letcher, M. Wigler, and F.S. Collins. 1990. The *NF1* locus encodes a protein functionally related to mammalian GAP and yeast *IRA* proteins. *Cell* **63:** 851–859.

Bar-Sagi, D. and J. Feramisco. 1985. Microinjection of the *ras* oncogene protein into PC12 cells induces morphological differentiation. *Cell* **42:** 841–848.

Basu, T.N., D.H. Gutmann, J.A. Fletcher, T.W. Glover, F.S. Collins, and J. Downward. 1992. Aberrant regulations of *ras* proteins in tumour cells from type 1 neurofibromatosis patients. *Nature* **356:** 713–715.

Bernards, A., A. Snijders, G.E. Hannigan, A.E. Murthy, and J.F. Gusella. 1993. Mouse neurofibromin type 1 cDNA sequence reveals high degree of conservation of both coding and noncoding mRNA segments. *Hum. Mol. Genet.* **2:** 645–650.

Bradley, A. 1987. *Production and analysis of chimeric mice.* IRL Press, Oxford, England.

Buchberg, A.M., L.S. Cleveland, N.A. Jenkins, and N.G. Copeland. 1990. Sequence homology shared by neurofibromatosis type-1 gene and *IRA-1* and *IRA-2* negative regulators of the *RAS* cyclic AMP pathway. *Nature* **347:** 291–294.

Cawthon, R.M., R. Weiss, G. Xu, D. Viskochil, M. Culver, J. Stevens, M. Robertson, D. Dunn, R. Gesteland, P. O'Connell, and R. White. 1990. A major segment of the Neurofibromatosis type 1 gene: cDNA sequence, genomic structure, and point mutations. *Cell* **82:** 193–201.

Cochard, P., M. Goldstein, and I.B. Black. 1978. Ontogenic appearance and disappearance of tyrosine hydroxylase and catecholamines in the rat embryo. *Proc. Natl. Acad. Sci.* **75:** 2986–2990.

Daston, M.M. and N. Ratner. 1992. Neurofibromin, a predominantly neuronal GTPase activating protein in the adult, is ubiquitously expressed during development. *Dev. Dynamics* **195:** 216–226.

Daston, M.M., H. Scrable, M. Nordlund, A.K. Sturbaum, L.M. Nissen, and N. Ratner. 1992. The protein product of the neurofibromatosis type 1 gene is expressed at highest abundance in neurons, schwann cells, and oligodendrocytes. *Neuron* **8:** 415–428.

DeClue, J.E., A.G. Papageorge, J.A. Fletcher, S.R. Diehl, N. Ratner, W.V. Vass, and D.R. Lowy. 1992. Abnormal regulation of mammalian $p21^{ras}$ contributes to malignant tumor

growth in von Recklinghausen (type 1) neurofibromatosis. *Cell* **69:** 265–273.

Golubic, M., M. Roudebush, S. Dobrowski, A. Wolfman, and D.W. Stacey. 1992. Catalytic properties, tissue and intracellular distribution of neurofibromin. *Oncogene* **7:** 2151–2160.

Gutmann, D.H. and F.S. Collins. 1993. The neurofibromatosis type 1 gene and its protein product, neurofibromin. *Neuron* **10:** 335–343.

Gutmann, D.H., L.B. Andersen, J.L. Cole, M. Swaroop, and F.S. Collins. 1993. An alternatively-spliced mRNA in the carboxy terminus of the neurofibromatosis type 1 (*NF1*) gene is expressed in muscle. *Hum. Mol. Genet.* **2:** 989–992.

Hall, A. 1990. *ras* and GAP-who's controlling whom? *Cell* **61:** 921–923.

Hogan, B., F. Constantini, and E. Lacy. 1986. *Manipulating the mouse embryo: A laboratory manual.* Cold Spring Harbor Laboratory, Cold Spring Harbor, New York.

Huynh, D.P., T. Nechiporuk, and S.M. Pulst. 1994. Differential expression and tissue distribution of type I and type II neurofibromins during mouse fetal development. *Dev. Biol.* **161:** 538–551.

Jenkins, N.A., N.G. Copeland, B.A. Taylor, and B.K. Lee. 1982. Organization, distribution, and stability of endogenous ecotropic murine leukemia virus DNA sequences in chromosomes of *Mus musculus*. *J. Virol.* **43:** 26–36.

Johnson, M.R., A.T. Look, J.E. DeClue, M.B. Valentine, and D.R. Lowy. 1993. Inactivation of the *NF1* gene in human melanoma and neuroblastoma cell lines without impaired regulation of GTP-Ras. *Proc. Natl. Acad. Sci.* **90:** 5539–5543.

Kaufman, R.L., A.F. Hartmann, and W.H. McAlister. 1972. *Birth defects: Original article series* **8:** 92–95.

Kirby, M.L., T.F. Gale, and D.E. Stewart. 1983. Neural crest cells contribute to normal aorticopulmonary septation. *Science* **220:** 1059–1061.

Knudson, A.G. 1971. Mutations and cancer: statistical study of retinoblastoma. *Proc. Natl. Acad. Sci.* **68:** 820–823.

Laird, P.W., A. Zijderveld, K. Linders, M.A. Rudnicki, R. Jaenisch, and A. Berns. 1991. Simplified mammalian DNA isolation procedure. *Nucleic Acids Res.* **19:** 4293.

Legius, E., D.A. Marchuk, F.S. Collins, and T.W. Glover. 1993. Somatic deletion of the neurofibromatosis type 1 gene in a neurofibrosarcoma supports a tumor suppressor gene hypothesis. *Nature Genet.* **3:** 122–126.

Luna, L.G. 1968. *Manual of histologic staining methods of the Armed Forces Institute of Pathology*, pp. 195–196. McGraw-Hill, New York.

Marchuk, D.A., A.M. Saulino, R. Tavakkol, M. Swaroop, M.R. Wallace, L.B. Andersen, A.L. Mitchell, D.H. Gutmann, M. Boguski, and F.S. Collins. 1991. cDNA cloning of the type 1 neurofibromatosis gene: Complete sequence of the *NF1* gene product. *Genomics* **11:** 931–940.

Marshall, C.J. 1991. Tumor suppressor genes. *Cell* **64:** 313–326.

Martin, G.A., D. Viskochil, G. Bollag, P.C. McCabe, W.J. Crosier, H. Haubruck, L. Conroy, R. Clark, P. O'Connell, R.M. Cawthon, M.A. Innis, and F. McCormick. 1990. The GAP-related domain of the neurofibromatosis type 1 gene product interacts with *ras* p21. *Cell* **63:** 84-3-849.

Nishi, T., P.S.Y. Lee, K. Oka, V.A. Levin, S. Tanase, Y. Morino, and H. Saya. 1991. Differential expression of two types of the neurofibromatosis type 1 (*NF1*) gene transcripts related to neuronal differentiation. *Oncogene* **6:** 1555–1559.

Noda, M., M. Ko, A. Ogura, D.-G. Liu, T. Amano, T. Takano, and Y. Ikawa. 1985. Sarcoma viruses carrying *ras* oncogenes induce differentiation-associated properties in a neuronal cell line. *Nature* **318:** 73–75.

Nordlund, M., X. Gu, M.T. Shipley, and N. Ratner. 1993. Neurofibromin is enriched in the endoplasm reticulum of CNS neurons. *J. Neurosci.* **13:** 1588–1600.

Riccardi, V.M. 1981. Von Recklinghausen neurofibromatosis. *N. Engl. J. Med.* **305:** 1617–1627.

Riccardi, V.M. 1991. Neurofibromatosis: Past, present and future. *N. Engl. J. Med.* **324:** 1283–1285.

Riccardi, V.M. and J.E. Eichner. 1986. *Neurofibromatosis: Phenotype, natural history and pathogenesis.* Johns Hopkins University Press, Baltimore, MD.

Robertson, E., A. Bradley, M. Kuehn, and M. Evans. 1986. Germline transmission of genes introduced into cultured pluripotent cells by retroviral vector. *Nature* **323:** 445–448.

Siracusa, L.D., L.B. Russell, N.A. Jenkins, and N.G. Copeland. 1987. Allelic variation within the *Emv-15* locus defines genomic sequences closely linked to the *agouti* locus on mouse chromosome 2. *Genetics* **117:** 85–92.

The, I., A.E. Murthy, G.E. Hannigan, L.B. Jacoby, A.G. Menon, J.F. Gusella, and A. Bernards. 1993. Neurofibromatosis type 1 gene mutations in neuroblastoma. *Nature Genet.* **3:** 62–66.

Thomas, K.R. and M.R. Capecchi. 1987. Site-directed mutagenesis by gene targeting in mouse embryo-derived stem cells. *Cell* **51:** 503–512.

Viskochil, D., A.M. Buchberg, G. Xu, R.M. Cawthon, J. Stevens, R.K. Wolff, M. Culver, J.C. Carey, N.G. Copeland, N.A. Jenkins, R. White, and P. O'Connell. 1990. Deletions and a translocation interrupt a cloned gene at the neurofibromatosis type 1 locus. *Cell* **62:** 187–192.

Wallace, M.R., D.A. Marchuk, L.B. Andersen, R. Letcher, H.M. Odeh, A.M. Saulino, J.W. Fountain, A. Brereton, J. Nicholson, A.L. Mitchell, B.H. Brownstein, and F.S. Collins. 1990. Type 1 neurofibromatosis gene: Identification of a large transcript disrupted in three NF1 patients. *Science* **249:** 181–186.

Wright, L.L., T.J. Cunningham, and A.J. Smolen. 1983. Developmental neuron death in the rat superior cervical sympathetic ganglion: Cell counts and ultrastructure. *J. Neurocytol.* **12:** 727–738.

Xu, G., B. Lin, K. Tanaka, D. Dunn, D. Wood, R. Gesteland, R. White, R. Weiss, and F. Tamanoi. 1990a. The catalytic domain of the neurofibromatosis type 1 gene product stimulates *ras*GTPase and complements *ira* mutants of S. cerevisiae. *Cell* **63:** 835–841.

Xu, G., P. O'Connell, D. Viskochil, R. Cawthon, M. Robertson, M. Culver, D. Dunn, J. Stevens, R. Gesteland, R. White, and R. Weiss. 1990b. The neurofibromatosis type 1 gene encodes a protein related to GAP. *Cell* **62:** 599–608.

Targeted disruption of the neurofibromatosis type-1 gene leads to developmental abnormalities in heart and various neural crest-derived tissues.

C I Brannan, A S Perkins, K S Vogel, et al.

Genes Dev. 1994, **8:**
Access the most recent version at doi:10.1101/gad.8.9.1019